Lasers in Manufacturing Conference 2015

Adjustment and Impact of the Thermoplastic Microstructure of the Melting Layer in Laser-based Joining of Polymers to Metals

Klaus Schricker[a,*], Martin Stambke[a], Jean Pierre Bergmann[a]

[a] *Technische Universität Ilmenau, Department of Production Technology, Gustav-Kirchhoff-Platz 2, 98693 Ilmenau, Germany*

Abstract

In this paper, the influence of specific time-temperature parameters on the melting layer and mechanical properties is shown for laser-based joining of thermoplastics with metals. Based on a differential scanning calorimetry, the base material is characterized by parameters of melting temperature range and solidification range. These results were transferred to time-temperature profiles and correlated to the melting layer within the thermoplastic joining. Considering these results, the change in morphology and the influence on mechanical properties can be shown and correlated to fracture behavior within the plastic base material as well as the energy absorption of the joint during mechanical testing.

Keywords: joining, fundamentals and process simulation, metal-plastic hybrid Joints, thermal joining of polymers to metals

1. Introduction and State of the Art

The application of lightweight design in automotive industry, mechanical engineering and aviation industry requires a mass reduction without limiting the load capacity, stiffness or fatigue behavior of structural components. The use of new materials and multi-material-design enables functional lightweight constructions. Especially, the joining of thermoplastics to metals has a great potential in order to adapt construction materials to the local stress situation. However, combination of these dissimilar materials is a major challenge in terms of joining technologies. Thermal joining shows advantages over competitive

* Corresponding author. Tel.: +49-3677-69-3808; fax: +49-3677-69-1660
E-mail address: info.fertigungstechnik@tu-ilmenau.de

processes due to the lack of an additional material (e. g. adhesives) or a connecting element (e. g. screws or rivets) and enables a local and areal bonding with a high load capacity.

During the thermal joining process, the polymer gets molten by a heat flux, penetrates the surface structures and thus wets the metal surface. A permanent joint is formed after solidification. Based on this process, various energy sources, e. g. conductor (Sickert et al., 2014), inductor (Roesner et al., 2011), ultrasonic (Balle et al., 2012), resistance welding (Ageorges et al., 2006) or laser radiation (Katayama et al., 2012, Bergmann et al., 2012), can be used. Hence, the use of a laser based process shows advantages because of the beam shaping, e. g. rectangle or circular spot geometries, and thereof an adjustable temperature-time profile for the joining process and a locally limited energy input. The process can be performed as transmission joining (Arai et al., 2014) or heat conduction joining (Jung et al., 2013) for lap joints. In transmission joining, the laser beam passes through the thermoplastic joining partner and is absorbed at the boundary layer between metal and plastic. This leads to a high thermal load of the polymer at the contact area and requires a transmittance of the plastic material within laser wavelength. In heat conduction joining, the laser spot is targeted at the metal surface as upper joining partner and the heat is conducted through the metal sheet into the joining zone. This enables the processing of fiber reinforced plastics or non-transparent materials and induces a reduced thermal load of the plastic joining partner.

Starting from these process variations, a high strength of the joint requires a surface preparation of the metal partner and an adjusted process management for the joining process. Various investigations were carried out for corundum blasting in Bergmann et al., 2012, etching in Hino et al., 2011, laser processing in Amend et al., 2014, or machining in Cenigaonaindia et al., 2012. Independently from the structuring method, a high structure density and a surface morphology with sufficient undercuts showed the highest impact on joint strength. This behavior shifts the focus on the field of process management. Depending on a varied joining speed, three different fracture modes for thermoplastic-metal joints were identified in Wahba et al., 2011 (see Fig. 1) and categorized into interface fracture, mixed fracture and base plastic fracture. In these cases, the failure occurs within the boundary layer (a), the boundary layer plus base material (b) or the thermoplastic base material (c).

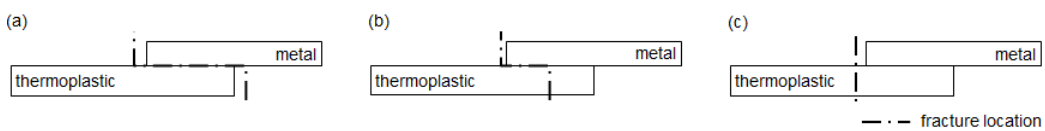

Fig. 1. (a) Interface fracture; (b) mixed fracture; (c) base plastic fracture according to Wahba et al., 2011

In case of base plastic failure, a correlation of material properties to failure behavior is not known yet. However, the joining process influences the polymers morphology within the joint zone and heat affected zone, as shown in Schricker et al., 2014 for spot joints of semi-crystalline PA 6.6 and aluminum. For laser welding of thermoplastics, Ghorbel et al., 2009 showed an analogous behavior for semi-crystalline polymers and Al-Wohoush et al., 2012 an impact on mechanical properties. Based on the materials science of polymers, a correlation between mechanical properties and morphology is shown in Osswald et al., 2012.

In this context, the impact of thermoplastics morphology, microstructural effects and process management for laser-manufactured metal-thermoplastic joints on mechanical properties is undetermined and will be investigated within this paper.

2. Experimental Proceeding

The experimental investigations were carried out on a 3-axis processing table and a fiber-coupled diode laser (Laserline LDM 3000, $\lambda = 980\ nm$, $P_{max} = 3\ kW$). As base materials, aluminum EN AW 6082 (t = 1.5 mm) and Polyamide 6.6 (PA 6.6, t = 2 mm) were used. The lap joint configuration for heat conduction joining is shown in Fig. 2 (a). In the joining process, the beam power was constant at 1 kW (dwell time at beginning: 8 s) and positioned in the middle of the overlap. A circular spot geometry (Fig. 2 (b)) with a diameter of 6 mm and a top-hat intensity distribution was used. The clamping device ensures a constant pressure of 0.5 $N \cdot mm^{-2}$ within the joining zone. The metal surface towards the boundary layer was prepared by a fiber laser (Rofin Powerline F20) before the joining process with linear structures in joining direction (structure density: 28 $lines \cdot mm^{-1}$, depth: 30 µm, width: 25 µm, Fig. 2 (c)). Based on this process, the joining speed v was varied on condition of a fully wetted joint zone to influence the melting layer and thermoplastic microstructure.

For temperature measurement, thermocouples (type K) with a diameter of 0.2 mm were positioned in the middle of the joining zone. The data were recorded by a Dewetron DEWE 800 system with a sampling rate of 100 Hz. The temperature curves are determined by means of at least three measurements. For the determination of mechanical properties, a tensile shear test (test speed: 240 $mm \cdot min^{-1}$, clamping length: 30 mm) was used and at least five specimens (width: 25 mm) for each parameter were taken out of the middle of the joint. Martens method according to VDI guideline 2616, 2012 (HM 0.01/30/60) was used for hardness testing. The measurement direction and strategy is shown in Fig. 2 (d). Microsections were cut out in the middle of the joint zone at $l = 50\ mm$ (Fig. 2 (a)). The thermoplastic morphology is shown at the melting layer maximum (A) and edge area (B) as seen in Fig. 2 (d). Differential interference contrast microscopy was used for analyzing the thermoplastic morphology and microstructure by preparing the microsections by sputtering with ionized argon. The melting layers were measured at the maximum thickness as shown in Fig. 2 (d).

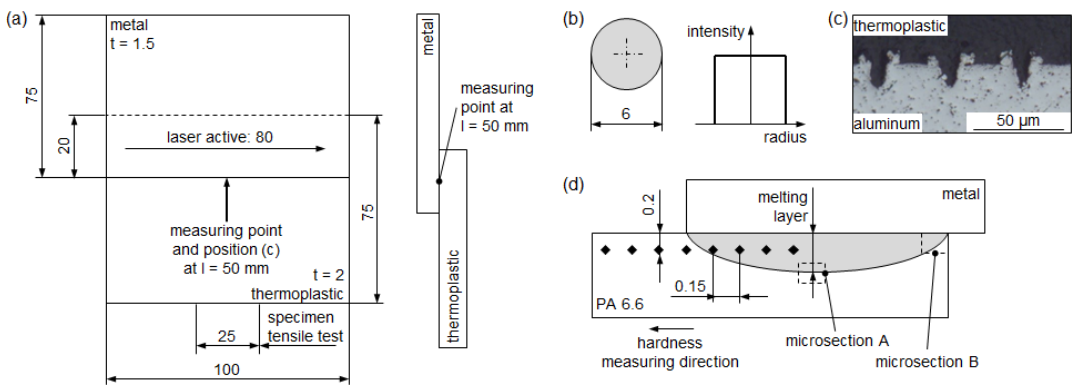

Fig. 2. (a) Joint geometry; (b) laser spot geometry; (c) surface preparation; (d) hardness measurement and microsection positions

A differential scanning calorimetry (DSC) was used for characterizing the PA 6.6 base material according to DIN EN ISO 11357-1 (Deutsches Insitut für Normung, 2010) with a heat rate of 10 $K \cdot min^{-1}$ for determining the melting and solidification range to derive the T_{im} (initial melting range) and T_{ic} (initial solidification range) parameters. The temperature range in DSC was from 25 °C to 300 °C to melt the polymer entirely and avoid decomposition due to higher temperatures.

The investigations are correlating material specific parameters with time-temperature profiles. This proceeding allows the process independent description of effects regarding morphology and mechanical behavior.

3. Results and Discussion

3.1. Characterization of the base material PA 6.6 and derivation of a relevant time-temperature interval

Based on differential scanning calorimetry, the time interval of molten polymer (Δt_l) between the temperatures of initial melting range T_{im} and initial solidification range T_{ic} can be determined (Fig. 3). The heating curve shows the non-homogeneous morphology of PA 6.6. Below the glass transition temperature T_g (about 85 °C), the movement of amorphous areas is frozen. Above T_g, crystallization of amorphous areas occurs which can lead to a heat affected zone with higher cristallinity within the joint. By increasing the temperature up to 240 °C, T_{im} is reached and crystalline lamellae smaller thicknesses get molten. At the end of the melting range (about 270 °C), all crystallites are molten. During the cooling curve, solidification of crystallites starts at $T_{ic} = 230$ °C. At 220 °C, the maximum crystallization rate is reached. Due to the one-sided, partially melting of the polymer within the joint zone, T_{im} and T_{ic} are defined as begin of the melting and solidification range in laser-based joining. It should be noted that the named temperatures are depending on heating and cooling rates, but provide a basis for analyzing the time-temperature profile.

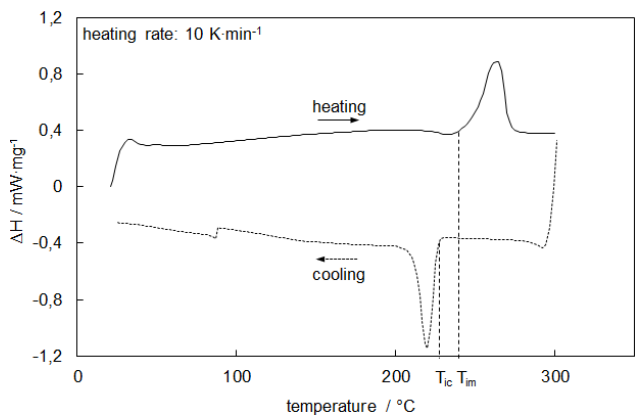

Fig. 3. Differential scanning calorimetry of PA 6.6 and derived temperature parameters T_{ic} and T_{im}

A transfer of these results to the time-temperature profile in laser-based joining is shown in Fig. 4 for a characteristic curve within the boundary layer, where the highest temperatures occur. The dashed rectangle signal (- - -) shows the active laser. In case of the described experimental setup, the temperature curve depends on the position of the moving laser spot, the dwell time (t_d) and joining speed. After starting the process, the temperature at the boundary layer increases up to a maximum of 379 °C when the laser passes the thermocouple. The maximum standard deviation follows the temperature maximum and is about ± 11 K. Afterwards, the temperature decreases and an inflection point within the temperature curve occurs after turning the laser off. The calculated time interval Δt_l begins at T_{im} and ends within the cooling phase at T_{ic}. In this example, a mean time interval Δt_l of 16.6 s ± 0.6 s is reached for molten polymer. Based on these results, the growth of the melting layer depending on joining speed and the time interval Δt_l can be examined further.

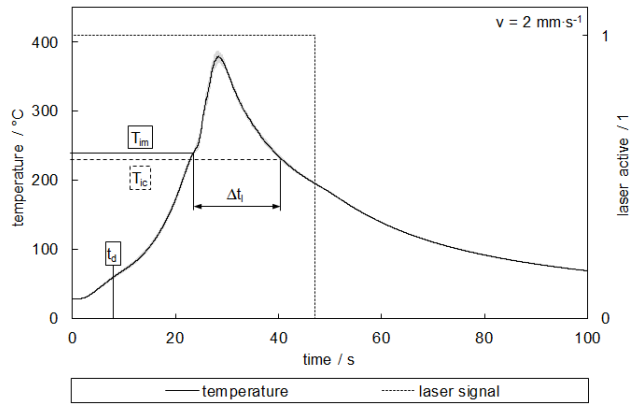

Fig. 4. Time-temperature profile of laser-based joining for joining speed 2 mm·s^{-1}

3.2. Melting layer in line joints

Based on these results, the interaction between joining speed and time interval Δt_l is examined. Fig. 5 (a) shows the correlation of Δt_l for a joining speed from 2 to 5 mm·s^{-1}. Joining speeds below 2 mm·s^{-1} caused a high thermal degradation. Furthermore, a joining speed above 5 mm·s^{-1} led to an insufficient wetting to the entire joining surface. Those parameters were not considered in this investigation and set up the limits of the process window. Thereby, Δt_l decreases continually from 16.6 s ± 0.6 s down to 5.9 s ± 0.8 s due to a reduced energy per unit length by increasing the joining speed from 2 up to 5 mm·s^{-1}. Hence, there is less time available for wetting the metal surface by molten plastic, whereby a modification of mechanical properties is expected.

Fig. 5 (b) shows the melting layer, characterized by the dimension of the maximum thickness (see Fig. 2 (d)) to quantify the molten polymer. By increasing the joining speed, the melting layer decreases from 530 µm ± 5.1 µm down to 266 µm ± 3.4 µm due to a reduced energy per unit length. The consolidation of the results allows a generalization based on the temperature-profile at the boundary layer, without considering laser beam power or joining speed as direct parameters.

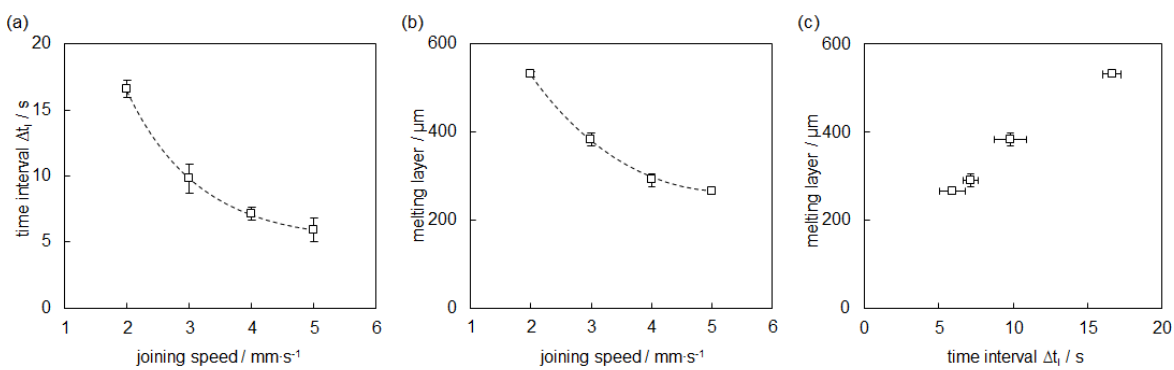

Fig. 5. (a) Correlation of Δt_l and joining speed; (b) correlation of melting layer and joining speed; (c) and consolidation of the results

Fig. 5 (c) shows the correlation of the time interval Δt_I and the melting layer thickness. For the observed times from 5.9 s up to 16.6 s, a nearly linear correlation between Δt_I and the resulting melting layer thickness can be assumed, but further investigations are necessary at this point. Thereby, the characterization of the melting layer by the maximum thickness and studies for longer times respectively a higher number of data points are the following objects of investigation.

In addition to the abovementioned time-dependent size of the melting layer, the thermoplastic morphology changed due to the time-temperature profile. Fig. 6 (a) shows the maximum of the melting layer (joining speed: 2 mm·s^{-1}) and four different areas: The molten zone (1), a transitional area of fine microstructure (2), a partially molten zone (3) and the base material (4) including the heat affected zone. In each zone, the time-temperature profile results in different effects on morphology and crystallinity. Firstly, the cooling rate adjusts nucleation rate which causally varies the size of microstructures as seen in (1) and (2). Secondly, the melting range (see 3.1) is not passed through completely and partially molten area occurs in zone (3). These areas can be deformed due to melt pool movement and ejection of the melt caused by the joining pressure at the lap joint edges (see zone (3) in Fig. 6 (c)). A comparable microstructure is given for higher joining speeds (see Fig. 6 (b, c)), although the areas show a smaller lateral extent. The above mentioned heat affected zone was examined on hardness testing for 2 and 5 mm·s^{-1}. A hardness gain up to 30 % within the heat affected zone starting from (3) towards (4) for both joining speeds was determined, but size determination of the heat affected zone requires a shorter distance between hardness indentations.

Based on these results, the influence of the varied morphology, melting layer and process influences, e. g. the ejection of the melt at the joint edge, on mechanical properties can be examined.

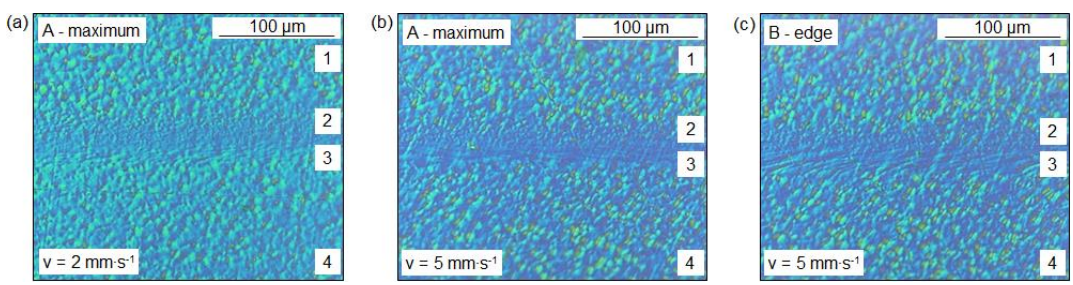

Fig. 6. Morphology of the melting layer: (a) maximum thickness (2 mm·s^{-1}); (b) maximum (5 mm·s^{-1}); (c) edge (5 mm·s^{-1})

3.3. Mechanical properties

The joints show varying mechanical properties depending on joining speed. In Fig. 7 (a), the joining speed is correlated to the reached force and crosshead travel in tensile shear testing. The mean force reaches its maximum at 4.2 kN for joining speeds from 4 mm·s^{-1} onwards. The lower forces and high standard deviations at 2 mm·s^{-1} and 3 mm·s^{-1} are caused by a failure at an early stage. By increasing the joining speed, the mean crosshead travel is advancing up to 20 mm, but with an enhanced spreading of the reached crosshead travel due to the ductile failure behavior.

The correlation of the time-temperature profile respectively the introduced time interval Δt_I is shown in Fig. 7 (b) for a generally relation of these results to the process. Despite the large standard deviation for low values of Δt_I, an exponential decrease in crosshead travel is shown for larger time intervals. The reason for

this behavior shown in Fig. 7 (a) and (b) is not yet answered definitely. Firstly, the change in reached crosshead travels depending on joining speed could be attributed to a higher cristallinity within the melting layer and heat affected zone, because crystalline areas show a decreased movability compared to amorphous areas. This effect could be explained by a large time interval Δt_I due to a slower solidification and a long-term heat treatment of the base material which causes a larger extend of the heat affected zone. Secondly, the varied microstructure within melting layer can cause a different fracture mode which goes beyond the degree of crystallization and shows the influence of crystalline structures, e. g. varied dimensions of the spherulites and a correlated change in mechanical behavior. Thirdly, the increase of molten material ejection by lower joining speeds could affect the crack-initiation and influence the fracture mode in combination with the high testing speed. Nevertheless, the fracture of the lap joint is always located within plastic base material.

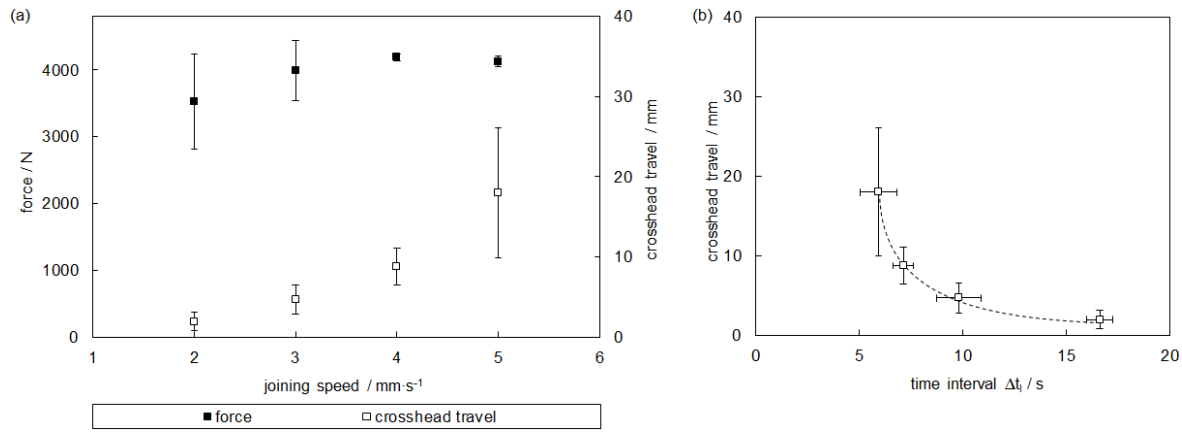

Fig. 7. Correlation between (a) joining speed and reached force in tensile shear test and (b) time interval Δt_I and reached crosshead travel

Concerning the fracture mode, characteristically force-crosshead travel graphs are shown in Fig. 8 (a) for the examined joining speeds. Comparable tensile shear forces were achieved for all shown samples. The rising crosshead travel by an increased joining speed is accompanied by necking within the Polyamide 6.6 which starts at the plateau after reaching the maximum force. Two examples of fractures are shown for 2 mm·s^{-1} and 5 mm·s^{-1} joining speed with a brittle respectively a ductile fracture in top view and in Fig. 8 (a). For 2 mm·s^{-1}, cracks towards the base material can be detected without necking of the specimen on reaching a crosshead travel of 1.5 mm. For 5 mm·s^{-1}, a ductile fracture with a clearly recognizable necking of the specimen reaches a crosshead travel of ca. 10 mm.

In Fig. 8 (b), microsections after tensile shear testing for both joining speeds are shown. The left pictures show each joint side, the right pictures each thermoplastic base material. For the brittle fracture (2 mm·s^{-1}), cracks can be detected outside the melt ejection (1), inside the melting layer at the joint edge as well as in base material (2). In contrast with a joining speed of 5 mm·s^{-1}, the crack at (3) only goes through the melting layer at the edge of the lap joint, shows a ductile fracture (4) and a deformed base material with reduced height due to necking towards base material. These microsections have to be seen as snapshots of these positions, but are leading to further questions concerning the transition of brittle to ductile fracture respectively the reached crosshead travel.

Potential starting points are the above mentioned arguments concerning a higher percentage of amorphous areas due to a higher cooling rate and varied time-temperature profile, a changed thermoplastic morphology respectively the heat affected zone. The influence of notch effects by the ejection of molten polymer, the crack initiation and crack propagation (e. g. inter-/transgranular) are additional questions. The clarification of these points would enable a mechanical characterization of hybrid joints based on material parameters and the time-temperature profile.

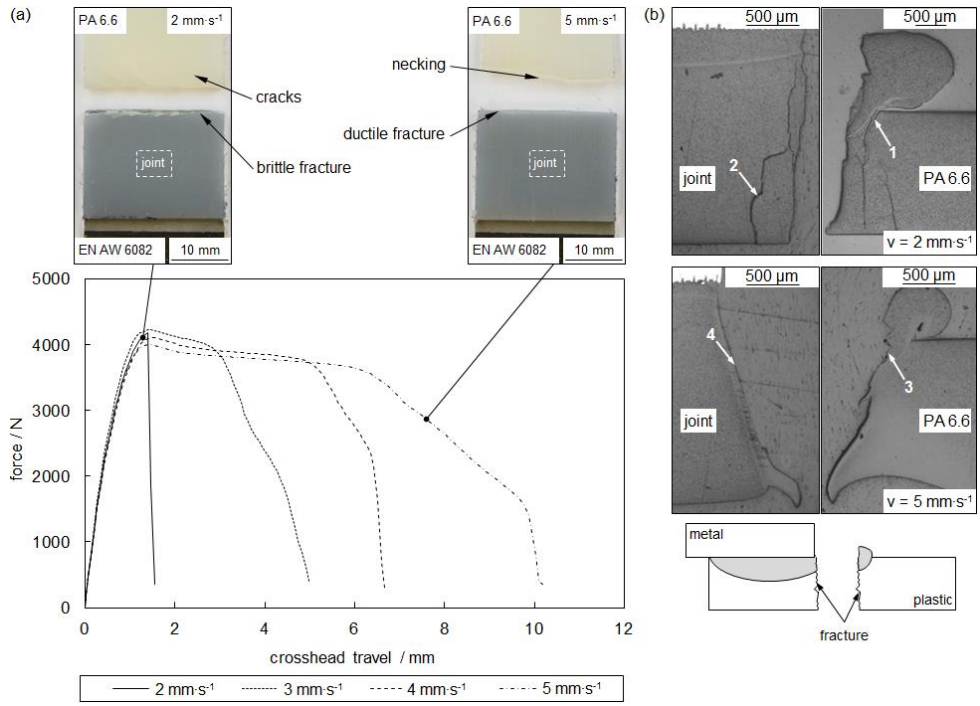

Fig. 8. (a) Characteristically force-crosshead travel graphs depending on joining speed; (b) fracture behavior

4. Summary and Outlook

In this paper, the correlation of material based parameters to specific time-temperature profiles is shown. The melting range and solidification range were identified by differential scanning calorimetry. The identified parameters T_{ic} and T_{im} were transferred to time-temperature profiles from measurements within the joint zone. The results were linked to a time-temperature profile depending interval Δt_l for molten polymer at the boundary layer and the correlation between melting layer and Δt_l is shown. Furthermore, the modification of the melting layer within plastic material was shown and characterized concerning to morphology and lateral extension.

By these results, a change in mechanical properties can be shown concerning the fracture behavior within the plastic base material as well as the energy consumption of the joint in mechanical testing. At this point, further investigations are necessary in order to correlate the ascertained morphology effects and process influences (e. g. ejection of molten polymer) to mechanical properties.

Acknowledgements

The authors would like to thank the Department of Economy, Employment and Technology (TMWAT) in Thuringia (Germany) and the European Social Fund (ESF) for the support of the project “Thermal Joining of Hybrid Structures” (“Thermisches Fügen von hybriden Materialkombinationen”) within the research group “Polymer Based Lightweight Composite Materials in Automotive Engineering” (“Kunststoffbasierte Leichtbauverbunde für Fahrzeuge”, Förderkennzeichen 2011FGR0109).

References

Sickert, M.; Haberstroh, E.; 2014. Thermal Direct Joining for Hybrid Plastic Metal Structures. Proceedings of Euro Hybrid Materials and Structures 2014, pp. 42-45.

Roesner, A.; Scheik, S.; Olowinsky, A.; Gillner, A.; Reisgen, U.; Schleser, M.; 2011. Laser Assisted Joining of Plastic Metal Hybrids. Physics Procedia 12, pp. 370-377.

Balle, F.; Eifler, D.; 2012. Monotonic and Cyclic Deformation Behavior of Ultrasonically Welded Hybrid Joints between Light Metals and Carbon Fiber Reinforced Polymers (CFRP). Fatigue Behaviour of Fiber Reinforced Polymers: Experiments and Simulations, DEStech Publications, pp. 111-122.

Ageorges, C.; Ye, L.; 2006. Resistance Welding of Metal/Thermoplastic Composite Joints. Journal of Thermoplastic Composite Materials, Vol. 14, No. 6, pp. 449-475.

Katayama, S.; Kawahito, Y.; Mizutani, M.; 2012. Latest progress in performance and understanding of laser welding. Physics Procedia 39, pp. 8-16.

Bergmann, J. P.; Stambke, M.; 2012. Potential of laser-manufactured polymer-metal hybrid joints. Physics Procedia 39, pp. 84-91.

Arai, S.; Kawahito, Y.; Katayama, S.; 2014. Effect of surface modification on laser direct joining of cyclic olefin polymer and steel. Materials and Design 59, pp. 448-453.

Jung, K.-W.; Kawahito, Y.; Takahashi, M.; Katayama, S.; 2013. Laser direct joining of carbon fiber reinforced plastic to aluminium alloy. Journal of Laser Applications, Vol. 25, No. 3, pp. 032003-1-032003-6.

Hino, M.; Mitooka, Y.; Murakami, K.; Urakami, K.; Nagase, H.; Kanadani, T.; 2011. Effect of Aluminum Surface State on Laser Joining between 1050 Aluminum Sheet and Polypropylene Resin Sheet Using Insert Materials. Materials Transactions, Vol. 52, No. 5, pp. 1041-1047.

Amend, P.; Mohr, C.; Roth, S.; 2014. Experimental Investigations of Thermal Joining of Polyamide Aluminium Hybrids Using a Combination of Mono- and Polychromatic Radiation. Physics Procedia 56, pp. 824-834.

Cenigaonaindia, A.; Liébana, F.; Lamikiz, A.; Echegoyen, Z.; 2012. Novel strategies for laser joining of polyamide and AISI 304. Physics Procedia 39, pp. 92-99.

Wahba, M.; Kawahito, Y.; Katayama, S.; 2011. Laser direct joining of AZ91D thixomolded Mg alloy and amorphous polyethylene terephthalate. Journal of Materials Processing Technology, pp. 1166-1174.

Schricker, K.; Stambke, M.; Bergmann, J. P.; 2015. Experimental Investigations and Modelling of the Melting Layer in Polymer-Metal Hybrid Structures. Welding in the World 59, DOI 10.1007/s40194-014-0213-0, pp. 407-412.

Ghorbel, E.; Casalino, G.; Abed, S.; 2009. Laser diode transmission welding of polypropylene: Geometrical and microstructure characterisation of weld. Materials and Design 30, pp. 2745-2751.

Al-Wohoush, M. H.; Kamal, M. R.; 2012. Characterization of Thermoplastic Laser-welded Joints. International Polymer Processing, Vol. 27, No. 5, pp. 574-583.

Osswald, T. A.; Menges, G.; 2012. Materials Science of Polymers for Engineers. 3rd edition, Hanser Publications, Cincinnati.

Verein Deutscher Ingenieure; Verband der Elektrotechnik, Elektronik und Informationstechnik, 2012. VDI/VDE 2616, Blatt 2: VDI/VDE Richtlinien. Härteprüfung an Kunststoffen und Elastomeren. Beuth Verlag, Berlin.

Deutsches Institut für Normung, 2010. DIN EN ISO 11357-1: Kunststoffe - Dynamische Differenz-Thermoanalyse (DSC) - Teil 1: Allgemeine Grundlagen. Beuth Verlag, Berlin.